

Image Decomposition Combining Staircase Reduction and Texture Extraction *

Tony F. Chan[†] Selim Esedoglu[†] Frederick E. Park[†]

March 23, 2005

Abstract

This paper proposes a natural and efficient way to achieve staircase reduction in texture extraction models of image processing. Moreover, we propose a precise framework for this amalgamation. In a sense, we utilize the best of both worlds: (I) the use of higher order derivatives through a variant of the Chambolle-Lions *inf convolution* energy (an image decomposition model in itself) along with (II) approximations to Meyer's G and E norms including the H^{-1} negative norm for ameliorating staircasing in image decomposition and restoration problems.

1 Introduction

The problem of texture and structure decomposition is an important image processing task that has seen much recent progress. In particular, much of this progress has been made through the use of nonlinear partial differential equations (PDEs) to model oscillating patterns which represent texture. In the seminal work [16], Meyer introduces the notion that image denoising can be thought of as image decomposition for the application of texture extraction. Furthermore, he introduces a variant of the popular model by Rudin, Osher, and Fatemi (ROF) [18] based on a space called the G space for this very purpose. The idea here is to replace the L^2 norm in the ROF model with a weaker norm that better captures textures or oscillating patterns. The G space that Meyer introduces is essentially the dual space of the space of functions of *bounded variation* (BV) and is defined as the space:

$$G = \{v \mid v = \partial_x g_1(x, y) + \partial_y g_2(x, y), \quad g_1, g_2 \in L^\infty(\Omega)\} \quad (1)$$

induced by the norm:

$$\|v\|_* = \inf_{\mathbf{g}=(g_1, g_2)} \left\{ \|\sqrt{g_1^2 + g_2^2}\|_{L^\infty} \mid v = \partial_x g_1 + \partial_y g_2 \right\}. \quad (2)$$

Here, $\Omega \subset \mathbb{R}^2$ is an open bounded domain (usually a rectangle in \mathbb{R}^2). Given a function f defined on Ω , Meyer's decomposition model then follows as:

$$\inf_u \left\{ E(u) = \int_{\Omega} |\nabla u| + \lambda \|v\|_*, \quad f = u + v \right\}. \quad (3)$$

*This work was partially supported by grants from the NSF under contracts DMS-9973341 and DMS-0410085, the ONR under contracts N00014-96-1-0277 and N00014-03-1-0888, and the NIH under contracts MH65166 and U54 RR021813.

[†]Department of Mathematics, University of California, 405 Hilgard Avenue, Los Angeles, CA 90095-1555. Email: {chan, esedoglu, fpark}@math.ucla.edu

In this model, the u component represents the structure or “cartoon” part of the image while the v component represents the texture part, thus, yielding the so called $u + v$ decomposition: $f = u + v$. It is shown numerically in [21, 17] that the $*$ norm indeed captures oscillatory patterns and texture better than the standard ROF model.

In practice, the model (3) is difficult to implement due to the nature of the $*$ norm. However, Vese and Osher [21] were the first to overcome this difficulty when they proposed an L^p approximation to the norm $\|\cdot\|_*$ in the following energy:

$$\inf_{u, g_1, g_2} \left\{ E_p(u, g_1, g_2) = \int_{\Omega} |\nabla u| + \lambda \int_{\Omega} |f - u - \partial_x g_1 - \partial_y g_2|^2 dx + \mu \left[\int_{\Omega} \left(\sqrt{g_1^2 + g_2^2} \right)^p dx \right]^{\frac{1}{p}} \right\}. \quad (4)$$

The first term enforces $u \in BV(\Omega)$ while the second and third terms enforce $\operatorname{div}(\mathbf{g}) \approx (f - u) \in G$. A central motivator for this energy is the L^p approximation to the L^∞ norm of $|\mathbf{g}| = \sqrt{g_1^2 + g_2^2}$, for $g_1, g_2 \in L^\infty(\mathbb{R}^2)$:

$$\|\sqrt{g_1^2 + g_2^2}\|_{L^\infty} = \lim_{p \rightarrow \infty} \|\sqrt{g_1^2 + g_2^2}\|_{L^p}. \quad (5)$$

In a subsequent work, Osher, Sole, and Vese (OSV) [17] consider using another L^p approximation to the norm: $\|\sqrt{g_1^2 + g_2^2}\|_{L^\infty}$ and choose $p = 2$ where they consider enforcing $|\mathbf{g}| \in L^2(\Omega)^2$ instead of $|\mathbf{g}| \in L^\infty(\Omega)$. It then follows that this particular approximation to the $*$ norm reduces to using the semi-norm in H^{-1} :

$$\|v\|_{H^{-1}(\Omega)}^2 = \int_{\Omega} |\nabla \Delta^{-1} v|^2 dx. \quad (6)$$

Consequently, a new image decomposition model based on the negative norm H^{-1} follows:

$$\inf_u \left\{ E(u) = \int_{\Omega} |\nabla u| + \lambda \|f - u\|_{H^{-1}(\Omega)}^2 \right\}. \quad (7)$$

The authors show that this new model (7) is simpler than the one introduced in (4) in the sense that there are fewer parameters to tune and only one unknown function to solve for. Moreover, arising from the Euler-Lagrange equations is an interesting new 4-th order PDE. Furthermore, they also go on to numerically show that the two models (4) and (7) have comparable texture removal properties and can both be seen as improvements to the ROF model for image decomposition and restoration problems.

Another approach used to solve Meyer’s original model is introduced by Aujol, Aubert, Blanc-Feraud, and Chambolle (AABC) [1] where the authors propose an approximation to (3) based on the discrete G norm:

$$\inf_{(u, v) \in \Omega \times \Omega} \left\{ J(u) + J^* \left(\frac{v}{\mu} \right) + \frac{1}{2\lambda} \int_{\Omega} (f - u - v)^2 dx \right\}. \quad (8)$$

In this energy, $J(u) = \int_{\Omega} |\nabla u|$ the TV norm of u and

$$J^* \left(\frac{v}{\mu} \right) = \begin{cases} 0 & \text{if } \frac{v}{\mu} \in B_G \\ +\infty & \text{otherwise} \end{cases} = \chi_{B_G} \left(\frac{v}{\mu} \right) \quad (9)$$

where $B_G = \{z \mid \|z\|_G \leq 1\}$. Moreover, the authors state that as $\lambda \rightarrow 0$ then $f \rightarrow u + v$ and (8) coincides with Meyer’s original model. Applications to non-textured SAR image restoration are provided. We will refer to (8) as the *AABC-G* approximation.

In the same spirit as in the above approach (8), Aujol and Chambolle (AC) [2] propose a $u + v$ image denoising method (v represents noise) based on the E space introduced by Meyer in [16] where

$E = B_{-1,\infty}^\infty$, the dual to the standard Besov space $B_{1,1}^1$. Meyer's E norm model is similar to his original model (3) except that the E norm replaces the $*$ norm and Aujol and Chambolle provide the following approximation to this variant:

$$\inf_{(u,v) \in \Omega \times \Omega} \left\{ J(u) + B^* \left(\frac{v}{\delta} \right) + \frac{1}{2\lambda} \int_{\Omega} (f - u - v)^2 d\mathbf{x} \right\}. \quad (10)$$

Here, $B^* \left(\frac{v}{\delta} \right) = \chi_{B_E} \left(\frac{v}{\delta} \right)$ where $B_E = \{z \mid \|z\|_E \leq 1\}$ and $J(u)$ is the standard TV norm as in (8). In this setting, the v component represents noise and the authors go on to numerically show that the approximation (10) is well suited to denoising textured images. We will refer to (10) as the AC - E approximation.

In addition to $u + v$ (structure + texture) decompositions, one can also consider introducing a noise component w , which leads to a $u + v + w$ decomposition consisting of structure, texture, and noise respectively. Recently, such a decomposition was introduced by Aujol and Chambolle (AC) in [2] which has the following formulation:

$$\inf_{(u,v,w) \in \Omega \times \Omega \times \Omega} \left\{ J(u) + J^* \left(\frac{v}{\mu} \right) + B^* \left(\frac{w}{\delta} \right) + \frac{1}{2\lambda} \int_{\Omega} (f - u - v - w)^2 d\mathbf{x} \right\}. \quad (11)$$

Here $J^* \left(\frac{v}{\mu} \right) = \chi_{\{v \mid \|v\|_G \leq \mu\}}$ and $B^* \left(\frac{w}{\delta} \right) = \chi_{\{w \mid \|w\|_E \leq \delta\}}$ are as in the above approximations (8) and (10) respectively. The key idea here is that the term $B^* \left(\frac{w}{\delta} \right)$ representing the E norm is used to model the noise in a given image for its tendency to preserve texture components when used with a fidelity term as in the approximation (10), see [2]. All the while, the term: $\left\{ J(u) + J^* \left(\frac{v}{\mu} \right) + \frac{1}{2\lambda} \int_{\Omega} (f - u - v - w)^2 d\mathbf{x} \right\}$ is an approximation to Meyer's original G model seen in (8). We will refer to model (11) as the AC - UVW model.

Many of the current PDE methods for image decomposition, including the aforementioned ones (4), (7), (8), (10), and (11), utilize TV regularization for its beneficial discontinuity (edge) preserving property. However, a particular caveat of such regularization is the staircasing effect in recovered images. Generally speaking, staircasing occurs most severely in image reconstructions by functionals that depend non-convexly on image gradients. A notable example is the Perona-Malik scheme which can be construed as gradient descent on a non-convex functional depending sublinearly on image gradients at infinity. The TV model is on the fringes of convexity; its dependence on image gradients is linear at infinity. This feature is a two edged sword since it is responsible for its ability to reconstruct images with discontinuities while also being responsible for staircasing. Some examples of staircasing in restorations from the ROF model can be seen in Figure 1. It will be shown in this paper that visually, staircase reduction is just as important a concept as that of the choice of appropriate norms for texture extraction. Thus, ameliorating staircasing should be considered a priority in image decomposition problems.

One way of overcoming staircasing in reconstructions from TV regularization is to introduce higher order derivatives into the energy. This approach is chosen by Chambolle and Lions (CL) [8], where they introduce the notion of *inf convolution* between two convex functionals. Here, an image u is decomposed into two parts: $u = u_1 + u_2$ where u_1 is measured with the TV norm and u_2 is measured using a higher order norm. Thus, the minimization problem follows as:

$$\inf_{u_1, u_2} \left\{ E(u) = \int_{\Omega} |\nabla u_1| + \alpha \int_{\Omega} |\partial^2 u_2| + \lambda \int_{\Omega} (f - u_1 - u_2)^2 d\mathbf{x} \right\}. \quad (12)$$

Minimizing this energy has the requisite that the discontinuous component of the image be allocated to the u_1 component while regions of moderate slopes are allocated to the u_2 component. Since the cost of regions of moderate but constant gradients is zero for the higher order norm, the allocation of

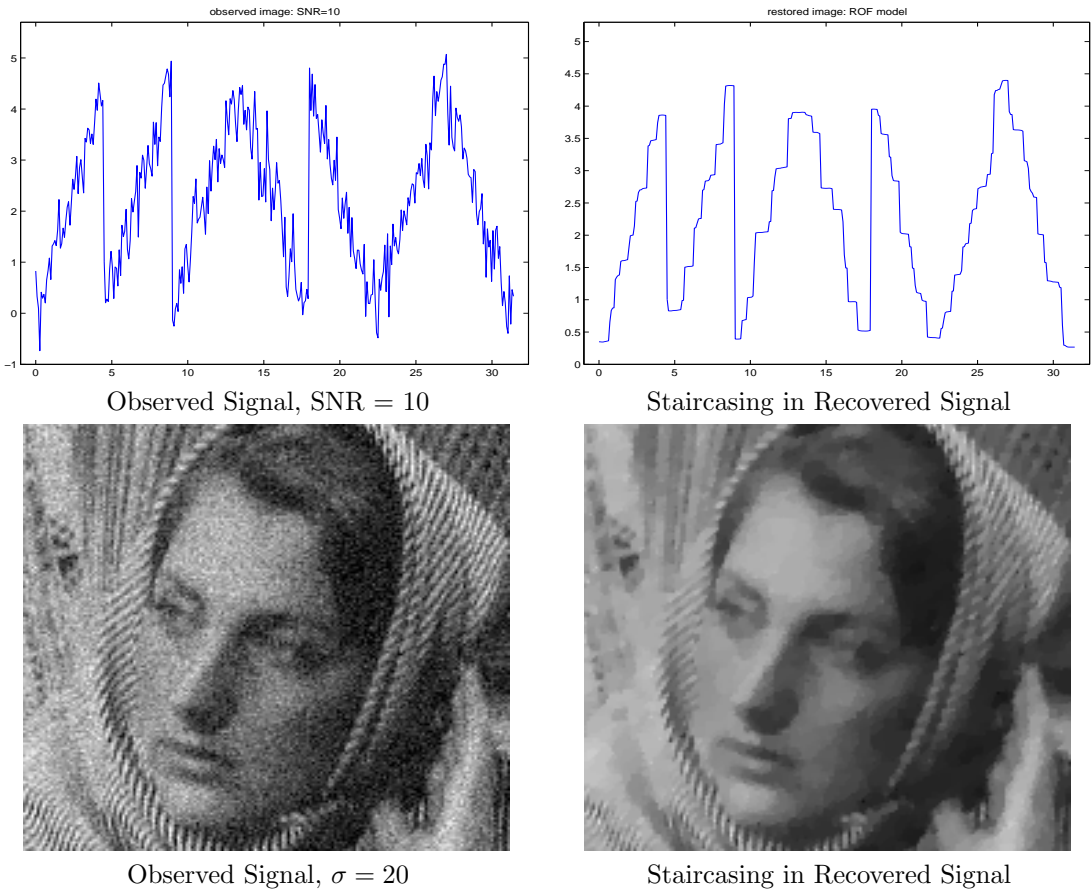


Figure 1: *Staircasing in Recovered Signals from the ROF Model*: Top left, observed 1-d signal, SNR=10. Bottom left, observed signal, $\sigma = 20$; σ^2 denotes the variance of the Gaussian noise. Top and bottom right, recovered signals from the ROF model [18]. Staircasing is observed in both recovered signals.

such regions to u_2 is of small cost. This model reduces staircasing to a remarkable degree in the 1-d examples presented in [8].

Blomgren, Mulet, Chan, and Wong [4] introduce another way of reducing staircasing in the model:

$$\inf_u \left\{ E(u) = \int_{\Omega} |\nabla u|^{L(|\nabla u|)} + \lambda(f - u)^2 dx \right\}. \quad (13)$$

Here, the function $L(\xi) : \mathbb{R} \rightarrow \mathbb{R}$ is chosen to monotonically decrease from 2 when $\xi = 0$, to 0 as ξ tends to infinity. The functional (13) is designed to be more convex in regions of moderate gradient (e.g. away from edges) and behave like the standard ROF model near discontinuities thus preventing staircasing.

The proposed framework naturally and efficiently amalgamates the two concepts of staircase reduction and texture extraction. We propose to incorporate a convex variant of the *inf convolution* of two convex functionals found in the CL energy (12) into approximations to the Meyer models. Thus, proving to be natural since both the variant and the CL model are already in decomposition form where

the CL model splits an image f into $f = u_1 + u_2 + v$ where u_1 , u_2 , v are the discontinuous, smooth, and noise components respectively. Moreover, such a combination will be shown to be efficient since solving for the additional smooth term u_2 in our variant amounts to solving a linear elliptic equation. This contrasts to the nonlinear 4-th order equation that results from the original CL model that is often restricted by a CFL condition. Numerical simulations will also be shown to demonstrate that (a) staircasing is clearly reduced, and that (b) the texture extraction properties of the Meyer norms will be preserved.

Some related works include, a decomposition model based on the anisotropic ROF model seen in [14] while another based on an L^1 fidelity term can be found in [9]. Two multiscale decompositions based on the TV model are introduced in [13, 20] while a simultaneous structure and texture image inpainting model is found in [3]. The closest related work is the interesting work by Levine et al. [15], where a model that combines the energy introduced by Blomgren, Mulet, Chan, and Wong (13) with a negative norm is introduced for image decomposition and restoration problems. One of the key differences between these two approaches is that the proposed functional in this paper is convex, whereas the one introduced in [15] is non-convex.

2 Proposed Model I: CEP- H^{-1} , U+V Decompositions

Higher order derivatives can easily be incorporated into the OSV model (7) to reduce staircasing from the TV norm. We propose to replace the TV term: $\int_{\Omega} |\nabla u|$ with the following energy: $\int_{\Omega} |\nabla u_1| + \alpha |\partial^2 u_2|$. Furthermore, we also make the modification that $u = u_1 + u_2$ in the fidelity term of (7) to arrive at the following model formulated as energy minimization:

$$\inf_{u_1, u_2} \left\{ E(u_1, u_2) = \int_{\Omega} |\nabla u_1| + \alpha |\partial^2 u_2| + \frac{1}{2\lambda} |\nabla(\Delta^{-1})(f - u_1 - u_2)|^2 d\mathbf{x} \right\}. \quad (14)$$

Here, f is the given observed image and as in the CL model (12), the energy term $\int_{\Omega} |\nabla u_1| + \alpha |\partial^2 u_2|$ is used to reduce the staircasing from the TV norm. In this context, u_1 contains the discontinuous component of the image f and u_2 contains the smooth component so that the structure component $u = u_1 + u_2$. The term involving the semi-norm in H^{-1} $\frac{1}{\lambda} \int_{\Omega} |\nabla(\Delta^{-1})(f - u_1 - u_2)|^2 d\mathbf{x}$ from the OSV model is used to better capture very oscillatory features in the texture component $v = f - u_1 - u_2$.

Instead of solving the original minimization in (14), we consider the slightly modified energy:

$$\inf_{u_1, u_2} \left\{ E(u_1, u_2) = \int_{\Omega} |\nabla u_1| + \frac{\alpha}{2} \int_{\Omega} |\Delta u_2|^2 d\mathbf{x} + \frac{1}{2\lambda} |\nabla(\Delta^{-1})(f - u_1 - u_2)|^2 d\mathbf{x} \right\} \quad (15)$$

where the term $|\Delta u_2|^2$ is an approximation to the term $|\partial^2 u_2|$ seen in (14). In fact, as is well known, the two terms $\int_{\Omega} |\partial^2 u|^2 d\mathbf{x}$ and $\int_{\Omega} |\Delta u|^2 d\mathbf{x}$ are identical on compactly supported smooth test functions:

$$\int_{\Omega} |\partial^2 u|^2 d\mathbf{x} = \int_{\Omega} |\Delta u|^2 d\mathbf{x} \quad \forall u \in C_c^2(\Omega).$$

This approximation allows for fast solvers for the smooth component u_2 while still maintaining the staircase reducing effects of the original model. In the latter claim, numerical results will be used to further justify this approach. We will refer to the model proposed in (15) as the CEP- H^{-1} model.

One way of minimizing the energy (15) is by solving the two coupled problems:

for u_2 fixed, solve:

$$\inf_{u_1} \left\{ \int_{\Omega} |\nabla u_1| + \frac{1}{2\lambda} \int_{\Omega} |\nabla \Delta^{-1}(f - u_1 - u_2)|^2 d\mathbf{x} \right\}, \quad (16)$$

for u_1 fixed, solve:

$$\inf_{u_2} \left\{ \frac{\alpha}{2} \int_{\Omega} |\Delta u_2|^2 d\mathbf{x} + \frac{1}{2\lambda} \int_{\Omega} |\nabla \Delta^{-1} (f - u_1 - u_2)|^2 d\mathbf{x} \right\}. \quad (17)$$

The discontinuous component u_1 can be obtained in two different manners. The first way is by driving the Euler-Lagrange equation of (16) to steady state:

$$\frac{\partial}{\partial t} u_1 = -\Delta \left[\operatorname{div} \left(\frac{\nabla u_1}{|\nabla u_1|} \right) \right] + \frac{1}{\lambda} (f - u_1 - u_2). \quad (18)$$

The second way of obtaining u_1 is introduced in [2] and follows a dual formulation of the OSV model. We first recall the dual form of the TV norm given in the following definition:

$$\int_{\Omega} |\nabla u| = \sup \left\{ \int_{\Omega} u(\mathbf{x}) \operatorname{div} \xi(\mathbf{x}) d\mathbf{x} \mid \xi \in C_c^1(\Omega; \mathbb{R}^2), |\xi(\mathbf{x})| \leq 1 \forall x \in \Omega \right\}. \quad (19)$$

Thus, we may define (16) as:

$$\inf_{u_1} \sup_{\xi} \left\{ \int_{\Omega} u_1 \operatorname{div} \xi d\mathbf{x} + \frac{1}{2\lambda} \int_{\Omega} |\nabla \Delta^{-1} (f - u_1 - u_2)|^2 d\mathbf{x} \mid \xi \in C_c^1(\Omega; \mathbb{R}^2), |\xi(\mathbf{x})| \leq 1 \forall x \in \Omega \right\}. \quad (20)$$

Swapping inf and sup and setting $v = \operatorname{div}(\xi)$ yields:

$$\sup_{v, v = \operatorname{div}(\xi)} \inf_{u_1} \left\{ \int_{\Omega} u_1 v d\mathbf{x} + \frac{1}{2\lambda} \int_{\Omega} |\nabla \Delta^{-1} (f - u_1 - u_2)|^2 d\mathbf{x} \mid \xi \in C_c^1(\Omega; \mathbb{R}^2), |\xi(\mathbf{x})| \leq 1 \forall x \in \Omega \right\}. \quad (21)$$

Then, for each v , the quantity

$$\inf_{u_1} \left\{ \int_{\Omega} u_1 v d\mathbf{x} + \frac{1}{2\lambda} \int_{\Omega} |\nabla \Delta^{-1} (f - u_1 - u_2)|^2 d\mathbf{x} \right\} \quad (22)$$

becomes defined point-wise for u_1 . Thus, for each v , minimizing said quantity yields a minimizer \tilde{u}_1 : $\tilde{u}_1 = f - u_2 + \lambda \Delta v$. Substituting this back into (21) and rewriting sup = -inf yields the following minimization with respect to v :

$$\inf_{v, v = \operatorname{div}(\xi)} \left\{ \int_{\Omega} (u_2 - f) v d\mathbf{x} + \frac{\lambda}{2} \int_{\Omega} |\nabla v|^2 d\mathbf{x} \mid \xi \in C_c^1(\Omega; \mathbb{R}^2), |\xi(\mathbf{x})| \leq 1 \forall x \in \Omega \right\} \quad (23)$$

and can be reformulated as:

$$\inf_{\xi} \left\{ \int_{\Omega} \nabla(f - u_2) \xi d\mathbf{x} + \frac{\lambda}{2} \int_{\Omega} |\nabla \operatorname{div}(\xi)|^2 d\mathbf{x} \mid \xi \in C_c^1(\Omega; \mathbb{R}^2), |\xi(\mathbf{x})| \leq 1 \forall x \in \Omega \right\}. \quad (24)$$

In the discrete setting, equation (24) can be set as a constrained minimization problem with inequality constraints:

$$\min_{p, |p| \leq 1} \left\{ \int_{\Omega} \nabla(f - u_2) p d\mathbf{x} + \frac{\lambda}{2} \int_{\Omega} |\nabla \operatorname{div}(p)|^2 d\mathbf{x} \right\} \quad (25)$$

whose Euler equation reads:

$$\nabla(f - u_2)_{i,j} + \lambda \nabla \Delta \operatorname{div}(p)_{i,j} + \alpha_{i,j} p_{i,j} = 0 \quad (26)$$

where the $\alpha_{i,j}$'s are the Lagrange multipliers for each i,j . Here, we would like to point out that the approach of solving a similar equation arising from the ROF model in the dual framework was pursued in [5, 11]. By the complementary slackness condition, either $\alpha_{i,j} = 0$ (where $\nabla(f - u_2)_{i,j} + \lambda \nabla \Delta \text{div}(p)_{i,j}$ is also 0) and $|p_{i,j}| < 1$ or $\alpha_{i,j} > 0$ and $|p_{i,j}| = 1$. Using the observation and essential contribution in [6], we see that in either case, the Lagrange multipliers are:

$$\alpha_{i,j} = |\nabla(f - u_2)_{i,j} + \lambda \nabla \Delta \text{div}(p)_{i,j}|$$

and the Euler equation (26) reduces to:

$$A_{i,j} + |A_{i,j}|p_{i,j} = 0$$

where $A_{i,j} = \nabla(\frac{f-u_2}{\lambda})_{i,j} + \nabla \Delta \text{div}(p)_{i,j}$. This equation can be solved by the semi-implicit fixed point (gradient descent) iteration scheme introduced in [2, 6]:

$$p^{n+1} = p^n - \tau (A_{i,j}^n + |A_{i,j}^n|p_{i,j}^{n+1})$$

where $A_{i,j}^n = \nabla(\frac{f-u_2}{\lambda})_{i,j} + \nabla \Delta \text{div}(p^n)_{i,j}$. Thus, the final iteration method reduces to:

$$p^0 = 0, \quad p_{i,j}^{n+1} = \frac{p_{i,j}^n - \tau \left(\nabla \left(\Delta \text{div}(p^n) + \frac{f-u_2}{\lambda} \right) \right)_{i,j}}{1 + \tau \left| \left(\nabla \left(\Delta \text{div}(p^n) + \frac{f-u_2}{\lambda} \right) \right)_{i,j} \right|}$$

where $f - u_2 + \lambda \Delta p^n \rightarrow \tilde{u}_1$ as $n \rightarrow \infty$ for τ small enough, with \tilde{u}_1 a solution to (16).

The smooth component u_2 can be obtained by solving the Euler-Lagrange equation from the minimization problem in (17):

$$\left(\frac{1}{\lambda} \Delta^{-1} - \alpha \Delta^2 \right) u_2 = \frac{1}{\lambda} \Delta^{-1} (f - u_1), \quad (27)$$

a linear elliptic PDE which can be solved fast via Fourier Analysis.

3 Proposed Models II: CEP-G and CEP-E, U+V Decompositions

We make a modification to the the model proposed by Meyer [16] to ameliorate the staircasing in the structure component $u = u_1 + u_2$, $f = u + v$ due to the TV reconstruction. Our proposed model II for $u + v$ decompositions then becomes a variation of Meyer's G norm model:

$$\inf_{f=u+v, u=u_1+u_2} \left\{ \int_{\Omega} |\nabla u_1| + \frac{\alpha}{2} \int_{\Omega} |\Delta u_2|^2 + \beta \|v\|_* \right\}. \quad (28)$$

We will refer to this model as the CEP-G model for the utilization of the G norm.

In practice, minimizing (28) is difficult due to the nature of the $*$ norm. Nonetheless, we may utilize a variant of the approximation proposed by Aujol et al. [1] to minimize said energy (28). Thus, our proposed approximation to (28) is called the CEP-G approximation:

$$\inf_{\{(u,v) \in \Omega \times \Omega, u=u_1+u_2\}} \left\{ \int_{\Omega} |\nabla u_1| + \frac{\alpha}{2} \int_{\Omega} |\Delta u_2|^2 + J^* \left(\frac{v}{\mu} \right) + \frac{1}{2\lambda} \int_{\Omega} (f - u_1 - u_2 - v)^2 dx \right\}. \quad (29)$$

Here, the term $\int_{\Omega} |\nabla u_1| + \frac{\alpha}{2} \int_{\Omega} |\Delta u_2|^2$ with $u = u_1 + u_2$, replaces the TV norm $\int_{\Omega} |\nabla u|$ to reduce staircasing in the structure component. The term $J^* \left(\frac{v}{\mu} \right) + \frac{1}{2\lambda} \int_{\Omega} (f - u_1 - u_2 - v)^2 dx$ with $J^* \left(\frac{v}{\mu} \right) = \chi_{\{v \mid \|v\|_G \leq \mu\}}$ remains almost as in the AABC-G approximation with the only difference being the additional u_2 component in the fidelity. As $\lambda \rightarrow 0$, using similar arguments as in [1], one can show that solving problem (29) yields a solution to the CEP-G model (28). Adopting the notation in [2], the discrete G space can be defined as:

$$G = \{v \in X \mid \exists g \in Y \text{ such that } v = \text{div}(g)\} \quad (30)$$

with norm

$$\|v\|_G = \inf \left\{ \|g\|_{\infty} \mid v = \text{div}(g), g = (g^1, g^2) \in Y, |g_{i,j}| = \sqrt{(g_{i,j}^1)^2 + (g_{i,j}^2)^2} \right\}. \quad (31)$$

We take for definition the set μB_G :

$$\mu B_G = \{v \in G \mid \|v\|_G \leq \mu\}. \quad (32)$$

One way of minimizing the energy (29) amounts to solving the following minimization problems:

for u_1 and v fixed, find solution u_2 of:

$$\min_{u_2} \left\{ \frac{\alpha}{2} \int_{\Omega} |\Delta u_2|^2 + \frac{1}{2\lambda} \int_{\Omega} (f - u_1 - u_2 - v)^2 dx \right\}, \quad (33)$$

for u_1 and u_2 fixed, find solution v of:

$$\min_{v \in \mu B_G} \left\{ \int_{\Omega} (f - u_1 - u_2 - v)^2 dx \right\}, \quad (34)$$

for u_2 and v fixed, find solution u_1 of:

$$\min_{u_1} \left\{ \int_{\Omega} |\nabla u_1| + \frac{1}{2\lambda} \int_{\Omega} (f - u_1 - u_2 - v)^2 dx \right\}. \quad (35)$$

A solution \tilde{u}_2 of (33) can be found by solving the linear elliptic equation:

$$\left(\Delta^2 + \frac{1}{\lambda} I \right) u_2 = \frac{1}{\lambda} (f - u_1 - v) \quad (36)$$

for which there are many efficient solution techniques, such as the fast Fourier transform. Minimizing (34) is equivalent to the following minimization problem:

for u_1 and u_2 fixed, find a solution v of:

$$\min_{\left\| \frac{v}{\mu} \right\|_G \leq 1} \left\{ \frac{1}{2} \int_{\Omega} (f - u - v)^2 dx \right\}. \quad (37)$$

One can get a handle on the G norm in the discrete setting since the constraint: $\left\| \frac{v}{\mu} \right\|_G \leq 1$ in the above minimization amounts to finding g such that $v = \mu \text{div}(g)$, $|g| \leq 1$. Thus, the problem in equation (37) amounts to solving the constrained minimization:

$$\min_{|p| \leq 1} \left\{ \frac{1}{2} \int_{\Omega} (f - u - \mu \text{div}(p))^2 dx \right\}. \quad (38)$$

The Euler equation for this problem reads:

$$-\nabla(\mu \operatorname{div}(p) - (f - u_1 - u_2))_{i,j} + \alpha_{i,j} p_{i,j} = 0.$$

Again, as in section §2 and in [2, 6], the Lagrange multipliers $\alpha_{i,j} = |\mu \operatorname{div}(p) - (f - u_1 - u_2)|_{i,j}$, and the Euler equation reduces to

$$-A_{i,j} + |A_{i,j}| p_{i,j} = 0$$

where $A_{i,j} = \left(\operatorname{div}(p) - \frac{f - u_1 - u_2}{\mu} \right)_{i,j}$. Once again, this equation can be solved by a semi-implicit fixed point (gradient descent) iteration:

$$p^0 = 0, \quad p_{i,j}^{n+1} = \frac{p_{i,j}^n + \tau A_{i,j}^n}{1 + |A_{i,j}^n|}$$

so that for τ small enough, $v^n = \mu \operatorname{div}(p^n) \rightarrow \tilde{v}$ as $n \rightarrow \infty$, where \tilde{v} is a solution to (37).

One way of minimizing (35) amounts to solving the dual formulation of this problem: for u_2 and v fixed, find solution u_1 of:

$$\min_{u_1} \sup_{\xi} \left\{ \int_{\Omega} u_1 \operatorname{div}(\xi) + \frac{1}{2\lambda} \int_{\Omega} (f - u - v)^2 d\mathbf{x} \mid \xi \in C_c^1(\Omega; \mathbb{R}^2), |\xi| \leq 1 \right\}. \quad (39)$$

Following the framework in [5, 11], we can rewrite the above problem as:

$$\sup_{\xi} \min_{u_1} \left\{ \int_{\Omega} u_1 \operatorname{div}(\xi) + \frac{1}{2\lambda} \int_{\Omega} (f - u - v)^2 d\mathbf{x} \mid \xi \in C_c^1(\Omega; \mathbb{R}^2), |\xi| \leq 1 \right\} \quad (40)$$

where for each ξ , the inner quantity $\min_{u_1} \left\{ \int_{\Omega} u_1 \operatorname{div}(\xi) + \frac{1}{2\lambda} \int_{\Omega} (f - u - v)^2 d\mathbf{x} \right\}$ is now defined point-wise with respect to u_1 . Thus, $u_1 = f - u_2 - v - \lambda \operatorname{div}(\xi)$, for each ξ and problem (40) is equivalent to:

$$\min_{\xi, |\xi| \leq 1} \left\{ \int_{\Omega} (\lambda \operatorname{div}(\xi) - (f - u_2 - v))^2 \right\}.$$

In the discrete setting, the above problem becomes a constrained minimization problem with inequality constraints. In this setting, if we let $\xi = p$, then the above equation has Euler equation:

$$-\nabla(\lambda \operatorname{div}(p) - (f - u_2 - v))_{i,j} + \alpha_{i,j} p_{i,j} = 0$$

where $\alpha_{i,j}$ are the Lagrange multipliers. Once again, using the observation and essential contribution in [6], the Lagrange multipliers $\alpha_{i,j} = \left| \nabla(\lambda \operatorname{div}(p) - (f - u_2 - v))_{i,j} \right|$. Then, the Euler equation reduces to

$$-A_{i,j} + |A_{i,j}| p_{i,j} = 0$$

where $A_{i,j} = \nabla \left(\operatorname{div}(p) - \frac{f - u_2 - v}{\lambda} \right)_{i,j}$. Again, this equation can be solved by a semi-implicit fixed point (gradient descent) iteration scheme:

$$p^0 = 0, \quad p_{i,j}^{n+1} = \frac{p_{i,j}^n + \tau A_{i,j}^n}{1 + |A_{i,j}^n|}$$

so that for τ small enough, $u_1^n = f - u_2 - v - \lambda \operatorname{div}(p^n) \rightarrow \tilde{u}_1$ as $n \rightarrow \infty$, where \tilde{u}_1 is a solution to (39).

Of course, we can also replace the G norm $\|\cdot\|_*$ in the above CEP-G model (28) with the E norm, $E = B_{-1,\infty}^\infty$ to arrive at:

$$\inf_{\{(u,v) \in \Omega \times \Omega, u=u_1+u_2\}} \left\{ \int_{\Omega} |\nabla u_1| + \frac{\alpha}{2} \int_{\Omega} |\Delta u_2|^2 + \beta \|v\|_E \right\}. \quad (41)$$

We will call this proposed model the *CEP-E* model.

Again, as in the G norm case, problem (41) cannot be solved directly due to the nature of the E norm. However, we may also utilize a variant of the approximation proposed by Aujol et al. [1] to minimize the above energy (41). Our proposed approximation then becomes the *CEP-E* approximation:

$$\inf_{\{(u,v) \in \Omega \times \Omega, u=u_1+u_2\}} \left\{ \int_{\Omega} |\nabla u_1| + \frac{\alpha}{2} \int_{\Omega} |\Delta u_2|^2 + B^* \left(\frac{v}{\delta} \right) + \frac{1}{2\lambda} \int_{\Omega} (f - u - v)^2 dx \right\}. \quad (42)$$

One way of minimizing the above energy (42) amounts to solving the following minimization problems:

for u_1 and v fixed, find solution u_2 of:

$$\min_{u_2} \left\{ \frac{\alpha}{2} \int_{\Omega} |\Delta u_2|^2 + \frac{1}{2\lambda} \int_{\Omega} (f - u - v)^2 dx \right\}, \quad (43)$$

for u_2 and v fixed, find solution u_1 of:

$$\min_{u_1} \left\{ \int_{\Omega} |\nabla u_1| + \frac{1}{2\lambda} \int_{\Omega} (f - u - v)^2 dx \right\}, \quad (44)$$

for u_1 and u_2 fixed, find solution v of:

$$\min_{v \in \delta B_E} \left\{ \int_{\Omega} (f - u - v)^2 dx \right\}. \quad (45)$$

Minimizing (43) and (44) follow in exactly the same manner as the methods used above in the CEP-G model (29). We use the same method as in [2] for finding a minimizer \tilde{v} of equation (45). Here, \tilde{v} can be given by $\tilde{v} = f - u_1 - u_2 - WST(f - u_1 - u_2, \delta)$, where *WST* stands for the wavelet soft thresholding algorithm given in [7] with threshold δ .

4 Proposed Model III: CEP-UVW, U+V+W Decompositions

In this section, we utilize the AC-UVW model (11) that decomposes a given image f into three components: $f = u + v + w$. The u and v components remain structure and texture respectively and the additional component w represents the noise. However, to reduce staircasing in the structure component u , we again introduce the energy: $\int_{\Omega} |\nabla u_1| + \frac{\alpha}{2} \int_{\Omega} |\Delta u_2|^2$ that further splits u into $u = u_1 + u_2$. Thus, the proposed decomposition model becomes:

$$\inf_{u_1, u_2, v, w} \left\{ \int_{\Omega} \left\{ |\nabla u_1| + \frac{\alpha}{2} |\Delta u_2|^2 \right\} + J^* \left(\frac{v}{\mu} \right) + B^* \left(\frac{w}{\delta} \right) + \frac{1}{2\lambda} \int_{\Omega} (f - u_1 - u_2 - v - w)^2 dx \right\}, \quad (46)$$

where $J^* \left(\frac{v}{\mu} \right)$ and $B^* \left(\frac{w}{\delta} \right)$ are defined as in model (29) and (42) respectively. We will refer to this proposed model as the *CEP-UVW* model.

One way of minimizing the CEP–UVW energy (46) amounts to solving the following minimization problems:

for u_1 , v and w fixed, find solution u_2 of:

$$\min_{u_2} \left\{ \frac{\alpha}{2} \int_{\Omega} |\Delta u_2|^2 + \frac{1}{2\lambda} \int_{\Omega} (f - u_1 - u_2 - v - w)^2 d\mathbf{x} \right\}, \quad (47)$$

for u_2 , v and w fixed, find solution u_1 of:

$$\min_{u_1} \left\{ \int_{\Omega} |\nabla u_1| + \frac{1}{2\lambda} \int_{\Omega} (f - u_1 - u_2 - v - w)^2 d\mathbf{x} \right\}, \quad (48)$$

for u_1 , u_2 and w fixed, find solution v of:

$$\min_{v \in \mu B_G} \left\{ \int_{\Omega} (f - u_1 - u_2 - v - w)^2 d\mathbf{x} \right\}, \quad (49)$$

for u_1 , u_2 and v fixed, find solution w of:

$$\min_{w \in \delta B_E} \left\{ \int_{\Omega} (f - u_1 - u_2 - v - w)^2 d\mathbf{x} \right\}. \quad (50)$$

A solution \tilde{u}_2 of (47) can be found by solving the linear elliptic equation:

$$\left(\Delta^2 + \frac{1}{\lambda} I \right) u_2 = \frac{1}{\lambda} (f - u_1 - v - w) \quad (51)$$

which can be solved by the fast Fourier transform. A solution \tilde{u}_1 of (48) can be found in almost the exact manner as in the CEP–G (29) solver for u_1 . If we set $A_{i,j} = \nabla \left(\text{div}(p) - \frac{f - u_2 - v - w}{\lambda} \right)_{i,j}$, then the semi-implicit fixed point iteration scheme:

$$p^0 = 0, \quad p_{i,j}^{n+1} = \frac{p_{i,j}^n + \tau A_{i,j}^n}{1 + |A_{i,j}^n|}$$

has the property that for τ small enough, $u_1^n = f - u_2 - v - w - \lambda \text{div}(p^n) \rightarrow \tilde{u}_1$ as $n \rightarrow \infty$. Again, a minimizer \tilde{v} of (49) can be found in almost the exact same way as in the CEP–G (29) solver for v . If we set $A_{i,j} = \left| \frac{f - u_1 - u_2 - w}{\mu} - \text{div}(p) \right|_{i,j}$, then the fixed point iteration:

$$p^0 = 0; \quad p_{i,j}^{n+1} = \frac{p_{i,j}^n + \tau A_{i,j}^n}{1 + |A_{i,j}^n|}$$

has the property that for τ small enough, $v^n = \mu \text{div}(p^n) \rightarrow \tilde{v}$ as $n \rightarrow \infty$. Finally, a minimizer \tilde{w} of (50) can be found by computing $\tilde{w} = f - u_1 - u_2 - v - \text{WST}(f - u_1 - u_2 - v, \delta)$ where $\text{WST}(f - u_1 - u_2 - v, \delta)$ is wavelet soft thresholding of $f - u_1 - u_2 - v$ with threshold δ (see [2, 7]).

5 Parameter Selection

Coupling the energy: $\int_{\Omega} \{ |\nabla u_1| + \alpha |\Delta u_2| \}$ with the Meyer models introduces an additional parameter α that controls the smoothness of the component u_2 in the structural part of the image u , $u = u_1 + u_2$. We have found that in practice, this parameter is not difficult to tune and one just needs to set $\alpha > 1$.

A possible explanation for this is that the semi-norm: $\int |\Delta u_2|^2$ measures zero for linear regions. Hence, the allocation of regions of moderate but constant slope comes at very little cost to this energy, making it less sensitive to these regions, and in return, less sensitive to α . In all of the proposed models in this paper, the parameter α has exhibited this beneficial insensitivity.

The parameters for the CEP- H^{-1} model (15) include α and λ . α is easily tuned by setting $\alpha > 1$, as addressed above. The parameter λ controls the amount of oscillatory features being extracted from a given image; the larger λ is, the more the geometric features in the component $u = u_1 + u_2$ will be averaged. The value of λ depends on how much texture is to be extracted and can be tuned by the user, depending on the texture properties of the image.

The parameters for the CEP-G approximation (29) include α , μ , and λ . As mentioned earlier, we simply set $\alpha > 1$. As for λ , convergence to the original model (28) is expected to take place as $\lambda \rightarrow 0$; thus, λ should be chosen as small as possible. The parameter μ is a little more difficult to tune since it controls the quantity of the G norm. The larger μ is, the more the information is averaged in the structural component $u = u_1 + u_2$, and the more texture is extracted. Again, this depends upon the texture properties of the image.

The parameters for the CEP-E approximation (42) include α , δ , and λ . Again, α is easy to tune and we set $\alpha > 1$. As for λ , once again, convergence to the original model (41) is expected to take place as $\lambda \rightarrow 0$; thus, λ should be chosen as small as possible. The parameter δ , in the case of denoising, controls the amount of noise removal and we can use the popular threshold $\sigma\sqrt{2\log(MN)}$ where $M \times N$ is the size of the image, see [7, 16, 19]. For better visual results, we adopt the approach chosen by Aujol and Chambolle [2] and introduce a weighting parameter η and set $\delta = \eta\sigma\sqrt{2\log(MN)}$. In practice, η is equal or slightly smaller than 1.

The parameters for the CEP-UVW model (46) are α , δ , μ , η , and λ respectively. The choices for these parameters follow the same guidelines as above for the CEP-G and CEP-E approximations (29) and (42) respectively.

6 Numerical Experiments

6.1 1-d Experiments

Since staircasing is often easier to see in the 1-d setting, we include some experiments to better illustrate this phenomenon. Staircasing is reduced to a remarkable degree in the 1-d examples presented by the authors in [8]. The purpose of the next experiments is to show that the effective staircase reducing properties of the CL model (12) carry over in the context of image decomposition when combined with suitable norms for texture removal like the G , E , or H^{-1} norms.

Figure 1 exhibits the staircasing effect. On the left a noisy signal and on the right the recovered denoised signal from the ROF model. Staircasing is observed in the recovered signal and illustrates this particular caveat of TV regularization.

This first experiment demonstrates how staircasing carries over into texture extraction problems and also shows how it can be alleviated with the proposed CEP- H^{-1} model while preserving the texture extraction properties of the H^{-1} norm. In Figure 2 left, a clean 1-d signal consisting of structure and texture is observed while on the right, a noisy version of this signal is also observed, the signal to noise ratio (SNR) is 10. Figure 3 exhibits on the left, the structure component u , $f = u + v$, of the image obtained from the OSV model (7) and on the right, the component $u = u_1 + u_2$ obtained from the proposed CEP- H^{-1} model (15). Clearly, staircasing is observed in the structure component obtained from the OSV model in regions away from the oscillations. These staircased regions starkly contrast with the smooth regions found in the clean image seen in Figure 2. In the solution obtained from the

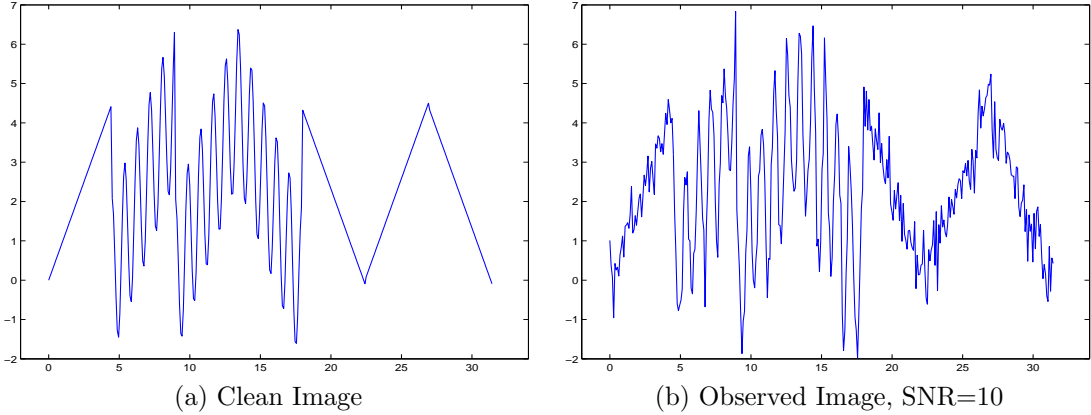


Figure 2: *Signal Containing Structure Texture and Noise*: A clean 1-d signal containing structure (ramps) and texture (oscillatory parts) is observed in (a). In (b), the same 1-d signal containing structure and texture is observed except in the presence of noise, SNR=10.

proposed model, the staircasing has been effectively reduced in the regions away from the oscillations and resembles more closely the smooth regions observed in the clean image in Figure 2.

The texture components v of these signals are comparable as demonstrated in Figure 4. Here, the component $v = f - u$ obtained from the OSV model is exhibited on the left while that of the proposed CEP- H^{-1} model, $v = f - u_1 - u_2$ is seen on the right. In both cases, the texture is effectively removed from the image and closely resemble each other. However, in the case of the proposed model, the texture is removed while resolving staircasing. Thus, staircase reduction seems to have no ill effects on the texture extraction properties of the H^{-1} norm.

In the 1-d experiments, for comparison purposes, the parameters for the OSV model (7) and the proposed CEP- H^{-1} (15) are chosen so that the L^2 norm of the texture components v have the same value.

6.2 2-d Experiments

In 1-d, both the proposed CEP- H^{-1} model and the CL model are effective at reducing staircasing in image reconstructions. The following experiments demonstrate that the modified energies incorporating higher order derivatives indeed capture texture as well as the non-modified ones and surpass the standard denoising models, while at the same time alleviating the staircasing phenomenon. For comparison purposes, the parameters for the models are chosen so that, in the case of $f = u + v$ models, the L^2 norm of the texture components v have the same value and in the case of $f = u + v + w$ models, the L^2 norm of the texture (v) + noise (w) have the same value.

The purpose of this first experiment is to show that staircasing can be resolved in the structure component u while not affecting the texture component v in the sense that the v component is comparable to current texture removal models, in particular the OSV model. In Figure 5(a), a clean 408×408 Barbara image containing both structure and texture parts is observed while Figure 5(b) exhibits a noisy version of the image with $\sigma = 20$, σ^2 the variance of the noise.

Figure 6 showcases the structure components: left, the OSV model (7) and right, the proposed CEP- H^{-1} model (15). Here, even without zooming, one can still detect some “terracing” in the u

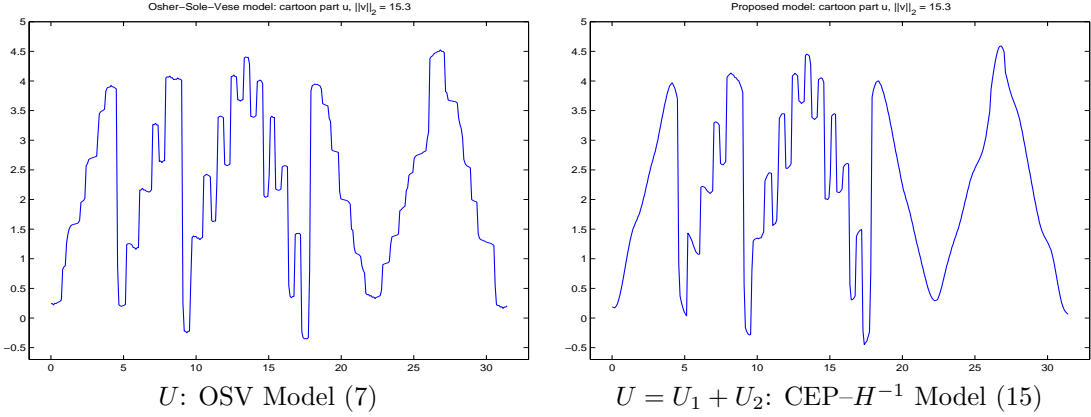


Figure 3: *Structure Components U , $f = U + V$ Decompositions*: Left, the structure component u , $f = u + v$ obtained from the OSV model. Staircasing is observed in regions away from the oscillations. These “terraced” regions starkly contrast to the piecewise linear regions in the clean image seen in Figure 2(a). Right, the structure component $u = u_1 + u_2$, $f = u + v$ obtained from the proposed CEP- H^{-1} model. Staircasing is greatly reduced in regions away from the oscillations and resemble more closely the piecewise linear regions in the clean image observed in Figure 2(a). The texture components v have $\|v\|_2 = 15.3$ for both models.

component obtained from the OSV model, particularly on the left side of the face (Barbara’s left) and her arms. The staircasing detected in the component from the OSV model has been successfully reduced in the component $u = u_1 + u_2$ obtained from the proposed model while still maintaining sharp edges. In the same ordering, the texture components are observed in Figure 7. On the left is the component $v = f - u + 150$ from the OSV model while on the right, the component $v = f - u_1 - u_2 + 150$ obtained from the proposed model. The texture components appear comparable with mostly texture (oscillating patterns) and very few structural (geometric) features visible. For example, the features of the face, arms, and hands of Barbara are almost nonexistent (as desired), only the oscillating patterns of texture from her pants, shawl, and hood along with the wicker patterns of the chair are visible. Thus, we conclude that staircase reduction in the structure component $u = u_1 + u_2$ from the proposed model does not affect the texture removal properties of the H^{-1} norm. The L^2 norm of the texture components v is $\|v\|_2 = 1662$ for both models.

Some zoom-ins of the structural (geometric) components found in 6 are shown in Figures 8 and 9 for comparison with the OSV model. In Figure 8 top left, we see the zoom-in of Barbara’s face from the OSV model. A large amount of staircasing is observed, particularly on the left side of Barbara’s face (her left). The same zoom-in of the face obtained from the proposed CEP- H^{-1} model is observed on the top right. Staircasing is reduced and the image has both smooth and discontinuous regions with a more natural appearance than image obtained from the OSV model. The same effects are observed in the images, bottom left and bottom right. In particular, in the region near the underarm, staircasing is observed in the component obtained from the OSV model and appears “terraced” and not natural. Once again, this phenomenon is reduced in the component from the proposed model. Observed in Figure 9 are more zoom-ins of the structure components found in Figure 6. Top and bottom left are from the OSV model. Top left, staircasing is observed on the hand while in the bottom left, “terracing” is observed on the forearm that looks almost scale-like. Top and bottom right, zoom-ins of the result from

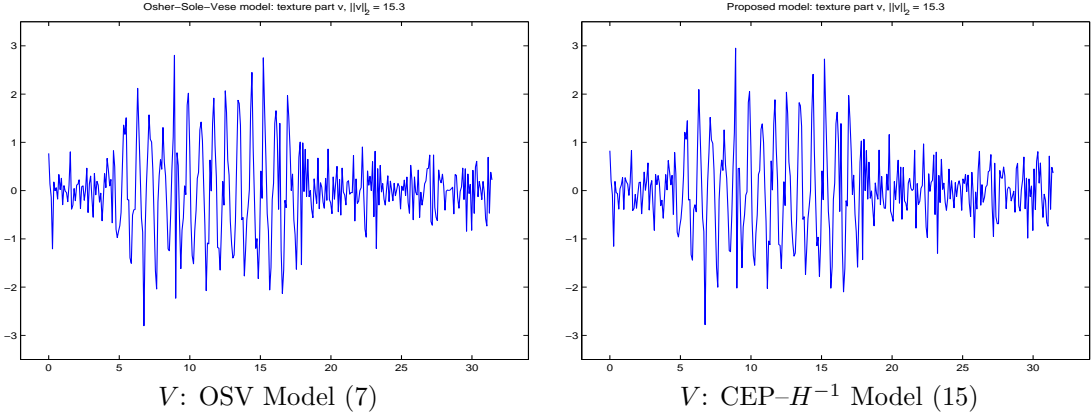


Figure 4: *Texture Components V , $f = U + V$ Decompositions*: Left, the texture component v , $f = u + v$ obtained from the OSV model. Right, the texture component v , $f = u_1 + u_2 + v$ obtained from the proposed CEP- H^{-1} model (15). Here, we make the observation that the models have comparable texture extraction properties even though staircasing is reduced in the component $u = u_1 + u_2$ obtained from the proposed model (15). In this experiment, we observe that staircase reduction does not affect the texture extraction properties of the negative norm.

the proposed model, staircasing has been successfully alleviated. We remind the reader that staircase reduction is accomplished with the proposed model while not affecting the texture removal properties of the negative norm. Thus, visually, staircase reduction makes a significant difference in the overall quality of the structural (geometric) components in the image decomposition.

We compare the proposed model with the standard denoising models, particularly the CL model, to ensure that the proposed CEP- H^{-1} model indeed captures texture better. In Figure 10 we observe the structure components obtained from, clockwise from top left, the OSV model, the ROF model, the CL model, and the proposed model. Even without zooming in, one can still detect staircasing in the u components obtained from the OSV and ROF models respectively. On the other hand, staircasing is resolved in the components $u = u_1 + u_2$ obtained from the C-L and proposed CEP- H^{-1} models. In all of the models, The texture is successfully removed from the given image, however, in the case of the CL and ROF models, some geometric features are also taken. In particular, in the components u and $u = u_1 + u_2$ from the ROF and Chambolle-Lions models respectively, many facial features are smeared out and not as well defined. These features are better preserved in the components u and $u = u_1 + u_2$ obtained from the OSV and proposed CEP- H^{-1} models respectively. Now, we consider the texture components v obtained from these models in Figure 11, with the same ordering. Here, we observe that all of the models successfully remove the texture from the Barbara image, however, more geometric features are observed in the texture components obtained from the ROF and CL models. In particular, more features from the face, arms, and hands are observed in these components. In the other hand, the texture components from the OSV and proposed CEP- H^{-1} models mostly contain oscillatory patterns and very little geometric features. From these experiments, we deduce that the proposed model removes texture cleaner than both the ROF and CL models. Moreover, the proposed and OSV models have comparable texture removal properties even though staircasing is ameliorated in the structural component $u = u_1 + u_2$ obtained from the proposed model.

The discontinuous and smooth structural components u_1 and u_2 from the proposed CEP- H^{-1} and



(a) Clean Barbara Image

(b) Observed Image, $\sigma = 20$

Figure 5: *Image Containing Structure, Texture, and Noise*: (a) Clean Barbara image containing structure and texture components. (b) Noisy observed image, $\sigma = 20$.

CL models are shown in Figure 12. More geometric features are observed in both components obtained from the proposed model. In particular, the facial features including Barbara’s eyes and mouth are better defined in both the smooth u_2 and discontinuous u_1 components obtained from the proposed model.

In the next experiment, we compare the AABC–G approximation (8) to the proposed CEP–G approximation (29). In Figure 13(a), a clean 311×311 Barbara image containing both structure and texture parts is observed while Figure 5(b) exhibits a noisy version of the image with $\sigma = 20$, σ^2 the variance of the noise. Figure 14 exhibits the structure components u for the AABC–G approximation (8) (left) and $u = u_1 + u_2$ for the proposed CEP–G approximation (29) (right). Without zooming in, staircasing can already be detected on the face (Barbara’s left side) and arms of the image obtained from the AABC–G approximation while these “terraced” regions are alleviated in the component obtained from the CEP–G approximation. In the same ordering, the texture components are observed in Figure 15 for both the AABC–G and the proposed CEP–G approximations. Comparable texture components v are observed even though staircasing is alleviated in the structure component $u = u_1 + u_2$ obtained from the proposed method. The L^2 norm of the texture components v is $\|v\|_2 = 1105$ for both methods.

For better visualization, in Figure 16, we display some zoom-ins of the structure components found in Figure 14. Top left we see the zoom-in of the face obtained from the AABC–G approximation (8) and a fair amount of staircasing is observed, particularly on the left side of the face (Barbara’s left). In the same zoom-in of the face obtained from the proposed CEP–G approximation (29), staircasing has been reduced. The same effects are observed in the images, bottom left and bottom right. Particularly in the region near the underarm where staircasing is observed in the component obtained from the AABC–G approximation while being reduced in the component obtained from the proposed approximation. The discontinuous and smooth components u_1 and u_2 from the proposed approximation are shown in Figure 17. From these experiments, we deduce that the proposed approximation removes texture comparably



U : OSV Model (7)



$U = U_1 + U_2$: CEP- H^{-1} Model (15)

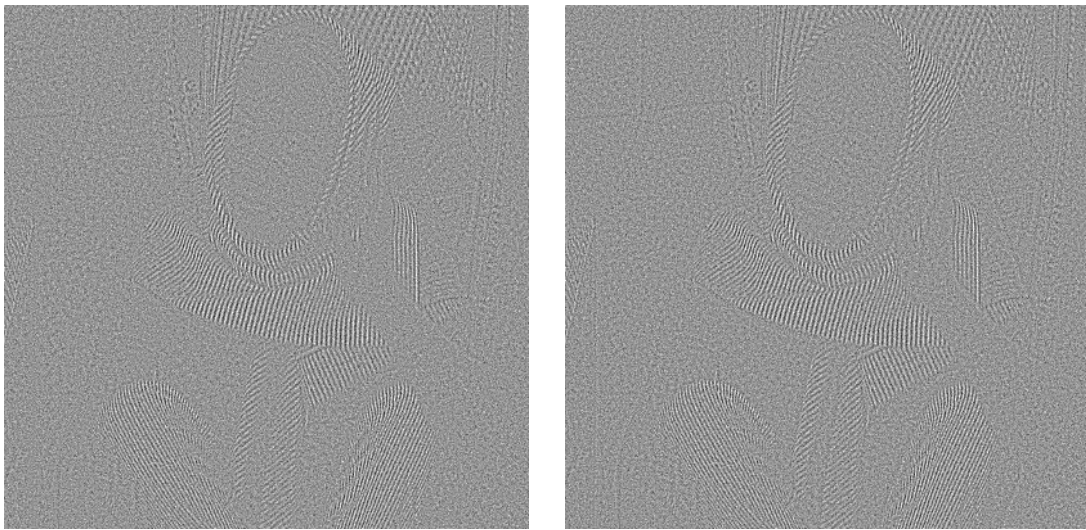
Figure 6: *Structure Components* U , $f = U+V$: Left, structure component u , $f = u+v$ obtained from the OSV model. Even without zooming, one can still detect some staircasing in this component, particularly on the left side of Barbara’s face (her left) and arms. Right, structure component $u = u_1 + u_2$, $f = u + v$ obtained from the proposed CEP- H^{-1} model (15). The staircasing detected in the component from the OSV model appears to have been reduced while sharp edges are still maintained. The texture components v have $\|v\|_2 = 1662$ for both models.

to the AC-G approximation while simultaneously ameliorating the staircase effect.

In this last experiment, we show that the same staircase reduction that occurs in the structure (u) + texture (v) case also takes place when modelling structure (u) + texture (v) + noise (w). In Figure 18 left, we observe the structure components from the AC-UVW model (11) and right, the proposed CEP-UVW model (46) obtained from the noisy image observed in Figure 13. Once again, as in the $f = u + v$ case, without zooming in, staircasing can already be detected on the face (Barbara’s left side) and arms of the image obtained from the AABC-UVW model. These “terraced” regions are alleviated in the component obtained from the proposed CEP-UVW model while maintaining sharp edges. For better visualization, a zoom-in of the same regions are exhibited in Figure 20 where similar conclusions are reached. Again, in Figure 19, the models exhibit comparable texture and noise decomposition properties even though staircasing is reduced in the structural (geometric) component $u - u_1 + u_2$ from the CEP-UVW model. For comparison purposes, the texture (v) + noise (w) components $v + w$ for both of the models have the same L^2 norm, $\|v + w\|_2 = 1057$.

7 Discussions and Future Works

In this paper, we proposed a natural and practical framework for reducing staircasing in image decomposition models, particularly in conjunction with the Meyer norms. Some future works include a fast solver for the term $\int_{\Omega} |\partial^2 u_1|$ (found in the original model by Chambolle and Lions [8]) when



V: OSV Model (7)

V: CEP- H^{-1} Model (15)

Figure 7: *Texture Components* V , $f = U + V$: Left and right, texture components $v + 150$ for the OSV model and the proposed model (15) respectively. Both models appear to have comparable texture extraction properties. Thus, staircase reduction in the structure component u from the proposed CEP- H^{-1} model does not affect the texture removal properties of the H^{-1} norm. The texture components v have $\|v\|_2 = 1662$ for both models.

amalgamated with texture extraction models in image processing.

Acknowledgements

The authors would like to thank Jean-Francois Aujol and David Weisbart for their valuable comments and discussions.

References

- [1] J.-F. Aujol, G. Aubert, L. Blanc-Feraud, A. Chambolle, Image decomposition: application to textured images and SAR images, Rapport de Recherche RR 4704, INRIA, January 2003.
- [2] J.-F. Aujol and A. Chambolle, Dual Norms and Image Decomposition Models, Intl. J. Comp. Vis. 63:1 (2005), pp. 85–104.
- [3] M. Bertalmio, L. Vese, G. Sapiro, and S. Osher, Simultaneous structure and texture image inpainting, IEEE Trans. Image Proc. 12:8 (2003), pp. 882–889.
- [4] P. Blomgren, P. Mulet, T. Chan, and C. Wong, Total variation image restoration: numerical methods and extensions, Proceedings ICIP (1997), pp. 384–387.
- [5] J. L. Carter, Dual methods for total variation-based image restoration, Ph.D. thesis (Advisor: T. F. Chan), UCLA (2001).

- [6] A. Chambolle, An algorithm for total variation minimization and applications, *JMIV* 20 (2004), pp. 89–97.
- [7] A. Chambolle, R. A. De Vore, N. Lee, B. J. Lucier, Nonlinear wavelet image processing: variational problems, compression, and noise removal through wavelet shrinkage. *IEEE Trans. Image Proc.* 7:3 (1998), pp. 319–335.
- [8] A. Chambolle and P. Lions, Image recovery via total variation minimization and related problems, *Numer. Math.* 76:2 (1997), pp. 167–188.
- [9] T. F. Chan and S. Esedoglu, Aspects of total variation regularized L^1 function approximation, *UCLA CAM Report 04-07* (2004), (Accepted for publication in *SIAM J. Appl. Math.*).
- [10] T. F. Chan, S. Esedoglu, and F. E. Park, A fourth order dual method for staircase reduction in texture extraction and image restoration problems, In Preparation (2005).
- [11] T. F. Chan, G. Golub, and P. Mulet, A nonlinear primal-dual method for total variation based image restoration, *SIAM J. Sci. Comp.*, 20 (1999), pp. 1964–1977.
- [12] T. F. Chan, A. Marquina, and P. Mulet, High order total variation based image restoration, *SIAM J. Sci. Comp.*, 22:2 (2000), pp. 503–516.
- [13] T. F. Chan and F. Park, Data Dependent multiscale total variation based image decomposition and contrast preserving denoising, *UCLA Cam Report 04-15* (2004).
- [14] S. Esedoglu and S. Osher, Decomposition of images by the anisotropic Rudin-Osher-Fatemi model, *Comm. Pure Appl. Math.* 57 (2004), pp. 1609–1626.
- [15] S. Levine, M. Ramsey, T. Misner, and S. Schwab, An adaptive model for image decomposition with applications to remote sensing, *Duquesne Univ. Dept. of Math and Comp. Sci. Tech. Report 05-01* (2005).
- [16] Y. Meyer, Oscillating patterns in image processing and nonlinear evolution equations (Lewis Memorial Lectures), *AMS* (2001).
- [17] S. Osher, A. Sole, and L. Vese, Image decomposition and restoration using total variation minimization and the H^{-1} norm, *Multiscale Model. Simul.* 1:3 (2003), pp. 349–370.
- [18] L. I. Rudin, S. Osher, and E. Fatemi, Nonlinear total variation based noise removal algorithms, *Physica D* 60 (1992), pp. 259–268.
- [19] J. L. Starck, M. Elad, and D. L. Donoho, Image decomposition: separation of texture from piecewise smooth content, *Proceedings SPIE 5207* (2003), pp. 571–582.
- [20] E. Tadmor, S. Nezzar, and L. Vese, A multiscale image representation using hierarchical (BV, L^2) decompositions, *Multiscale Model. Simul.* 2:4 (2003), pp. 554–579.
- [21] L. Vese and S. Osher, Modeling textures with total variation minimization and oscillating patterns in image processing, *J. Math. Imaging Vision* 20 (2004), pp. 7–18.



U : OSV Model (7)



$U = U_1 + U_2$: CEP- H^{-1} Model (15)



U : OSV Model (7)



$U = U_1 + U_2$: CEP- H^{-1} Model (15)

Figure 8: *Zoom-In of Structure Components U , $f = U + V$* : Left top and left bottom, zoom-in of the solution to the OSV model. Right top and right bottom, zoom-in of the solution to the proposed CEP- H^{-1} model (15). In the zoom-ins obtained from the OSV model, staircasing is observed on the left side of Barbara's face (her left) and arm affecting the quality of the image. In the zoom-ins obtained from the propose model, staircasing is ameliorated while maintaining sharp edges in the image.



U : OSV Model (7)



$U = U_1 + U_2$: CEP- H^{-1} Model (15)



U : OSV Model (7)



$U = U_1 + U_2$: CEP- H^{-1} Model (15)

Figure 9: *Zoom-In of Structure Components U , $f = U + V$* : Left top and left bottom, zoom-in of the solution to the OSV model. Right top and right bottom, zoom-in of the solution to the proposed CEP- H^{-1} model (15). Again, staircasing is observed in the zoom-ins obtained from the OSV model. This is particularly noticeable on the hand and forearm where a scale-like appearance occurs. In the same zoom-ins from the proposed model, staircasing has been ameliorated while maintaining sharp edges.



U : OSV Model (7)



U : Standard ROF Model

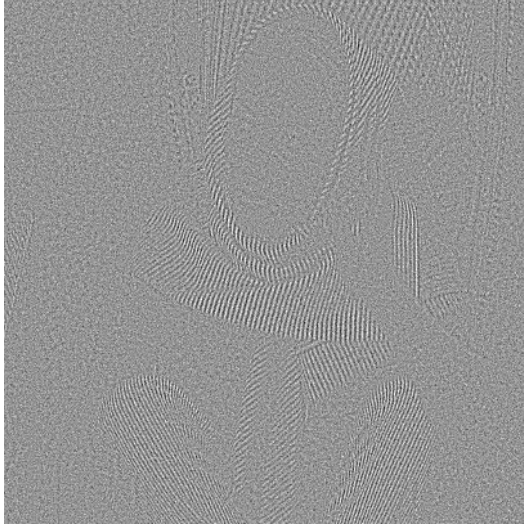


$U = U_1 + U_2$: CEP- H^{-1} Model (15)



$U = U_1 + U_2$: CL Model (12)

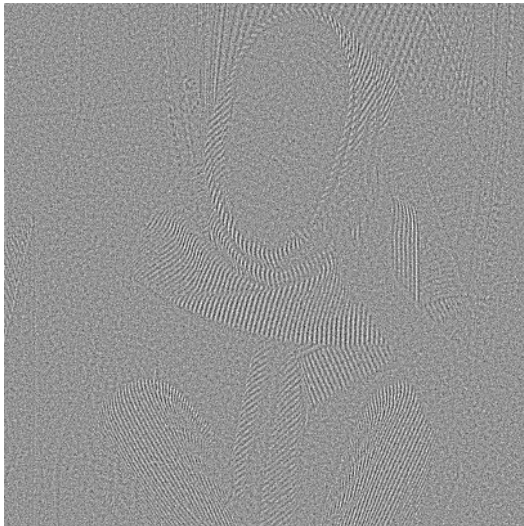
Figure 10: *Comparison of Structure Components U , $f = U + V$* : Clockwise, from top left: structure components u obtained from the OSV, ROF, CL, and proposed CEP- H^{-1} models. More geometrical features are observed in the components obtained from the OSV and proposed models. This behavior is expected since the H^{-1} norm has the beneficial property that it tends to preserve such features while extracting texture. The components obtained from the ROF and CL models have less geometrical features since the standard L^2 fidelity term does not isolate the texture features as well as the H^{-1} norm. Moreover, some staircasing can also be detected in the components obtained from the OSV and ROF models. The parameters have been tuned in all of the models such that the L^2 norm of the texture components are the same, $\|v\|_2 = 1662$.



V: OSV Model (7)



V: Standard ROF Model



V: CEP- H^{-1} Model (15)



V: CL Model (12)

Figure 11: *Comparison of Texture Components V , $f = U + V$* : Clockwise, from top left: Texture components v obtained from the OSV, ROF, CL, and proposed CEP- H^{-1} models. The components obtained from the OSV and Proposed models have cleanly isolated the texture with few geometric features visible. This is expected since the H^{-1} norm tends to better extract such oscillatory features. The texture is also extracted in the components obtained from the CL and ROF models, however, more geometrical features are observed and the texture is not as well isolated. This behavior is expected since the ROF and CL models use a standard L^2 fidelity term that does not isolate oscillatory features as well. The parameters have been tuned in all of the models such that $\|v\|_2 = 1662$.



U_1 : CEP- H^{-1} Model (15)



U_2 : CEP- H^{-1} Model (15)



U_1 : CL Model (12)



U_2 : CL Model (12)

Figure 12: *Discontinuous and Smooth Components U_1 and U_2 , $U = U_1 + U_2$, $f = U + V$* : Top left and top right, discontinuous and smooth components $u_1 + 150$ and u_2 respectively from the proposed CEP- H^{-1} model (15). Bottom left and bottom right, discontinuous and smooth components $u_1 + 150$ and u_2 respectively obtained from the CL model (12). More features are observed in the components u_1 and u_2 obtained from the proposed model versus those obtained from the C-L model. For example, the facial features seem better defined in the components from the proposed model. The texture components v for both of the models have the same L^2 norm, $\|v\|_2 = 1662$.



(a) Clean Barbara Image



(b) Observed Image, $\sigma = 20$

Figure 13: *Images Containing Structure, Texture, and Noise:* (a) Clean Barbara image containing structure and texture components. (b) Noisy observed image, $\sigma = 20$.

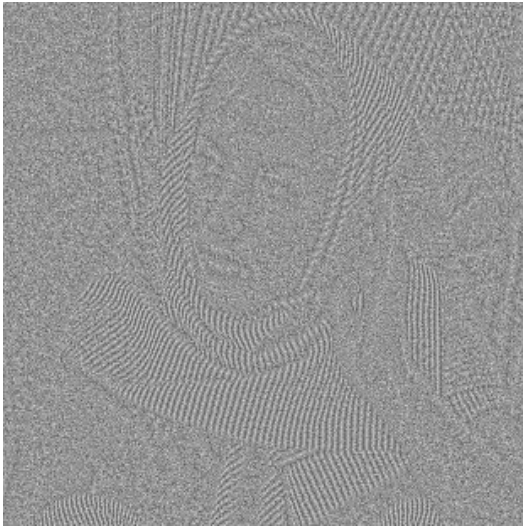


U : AABC-G Approximation (8)

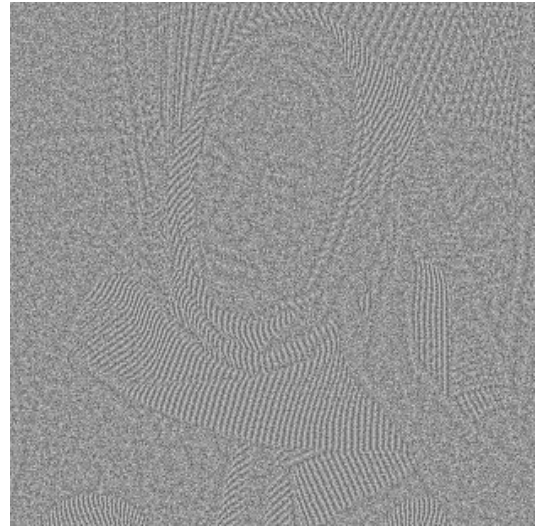


$U = U_1 + U_2$: CEP-G Approximation (29)

Figure 14: *Structure Components U , $f = U + V$:* From left to right, structure components u for the AABC-G approximation (8) and proposed CEP-G approximation (29) respectively. Without zooming in, staircasing can already be detected on the face (Barbara's left side) and arms of the image obtained from the AABC-G approximation. These "terraced" regions are alleviated in the component obtained from the proposed approximation. The texture components v for both methods have the same L^2 norm, $\|v\|_2 = 1105$.



V : AABC-G Approximation (8)



V : CEP-G Approximation (29)

Figure 15: *Texture Components V , $f = U + V$* : Left and right, texture components $v + 150$ for the AABC-G approximation (8) and the proposed CEP-G approximation (29) respectively. Both methods appear to have comparable texture extraction properties even though staircasing is reduced in the structure component u obtained from the proposed approximation. Here, we observe that staircase reduction does not affect the texture removal properties of the G norm. Parameters have been tuned in both methods such that the L^2 norm of the texture components are the same, $\|v\|_2 = 1105$.



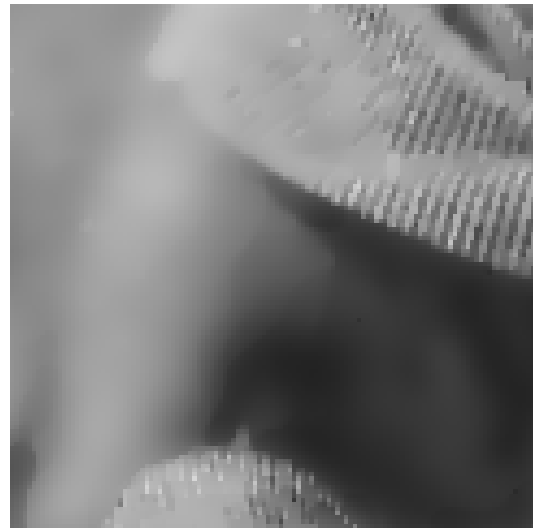
U : AABC-G Approximation (8)



$U = U_1 + U_2$: CEP-G Approximation (29)



U : AABC-G Approximation (8)

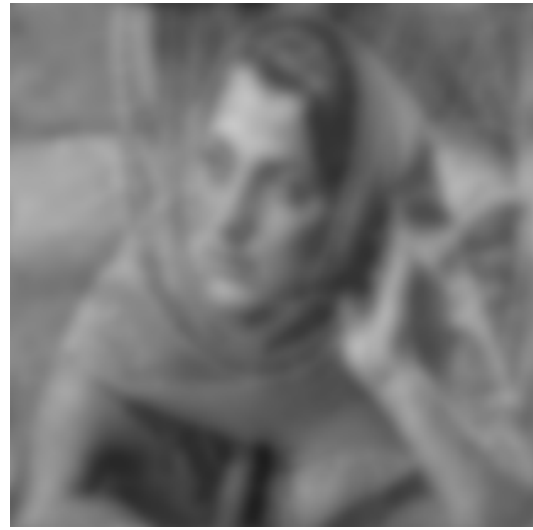


$U = U_1 + U_2$: CEP-G Approximation (29)

Figure 16: *Zoom-In of Structure Components U , $f = U + V$* : Left top and left bottom, zoom-in of the solution to the AABC-G approximation (8). Right top and right bottom, zoom-in of the solution to the proposed CEP-G approximation (29). Staircasing is observed in the components from the AABC-G approximation (8) while being ameliorated in the component obtained from the proposed approximation. This is particularly noticeable on the left side of Barbara's face (her left) and arm.



U_1 : CEP-G Approximation (29)



U_2 : CEP-G Approximation (29)

Figure 17: *Discontinuous and Smooth Components U_1 and U_2 , $U = U_1 + U_2$, $f = U + V$* : Left and right, the discontinuous and smooth components $u_1 + 150$ and u_2 respectively obtained from the proposed CEP-G approximation (29).

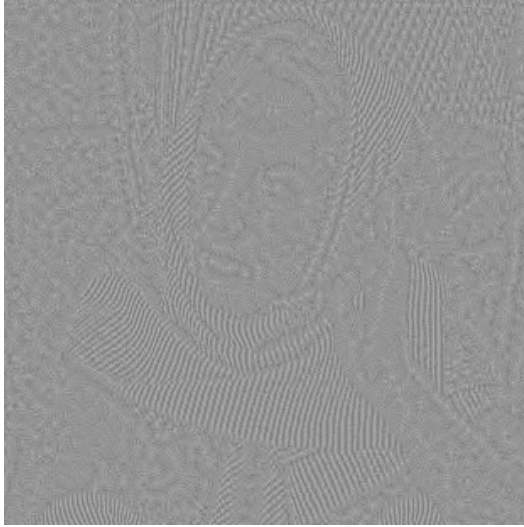


U : AC-UVW Model (11)

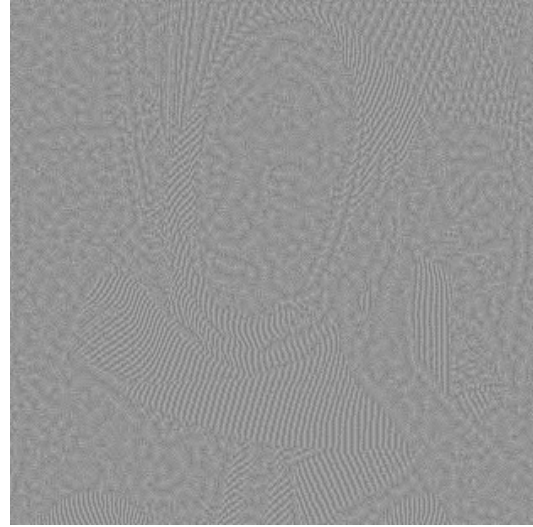


$U = U_1 + U_2$ CEP-UVW Model (46)

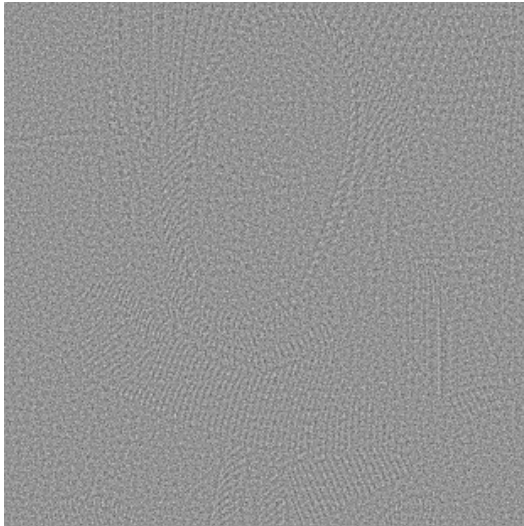
Figure 18: *Structure Components U , $f = U + V + W$* : From left to right, structure components u for the AC-UVW model (11) and $u = u_1 + u_2$ for the proposed CEP-UVW model (46) respectively. Again, as in the $f = u + v$ model case, without zooming in, staircasing can already be detected on the face (Barbara’s left side) and arms of the image obtained from the AC-UVW model. These “terraced” regions are alleviated in the component obtained from the proposed model while sharp edges are still maintained. The texture (v) + noise (w) components for both models have the same L^2 norm, $\|v + w\|_2 = 1057$.



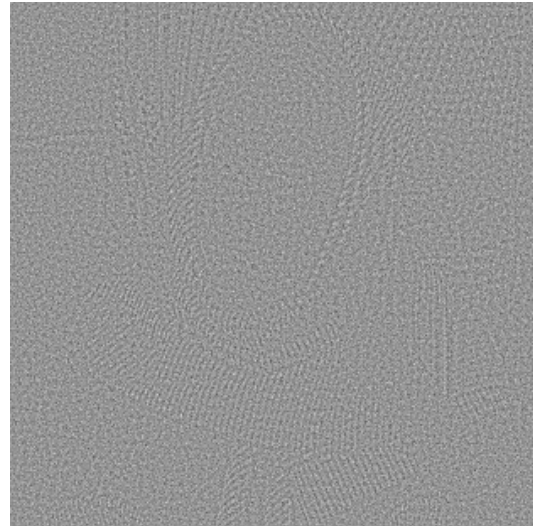
V: AC-UVW Model (11)



V: CEP-UVW Model (46)



W: AC-UVW Model (11)



W: CEP-UVW Model (46)

Figure 19: *Texture V and Noise W Components, $f = U + V + W$* : Top left and top right, texture components $v + 150$ for the AC-UVW (11) and proposed CEP-UVW (46) models respectively. Bottom left and bottom right, noise components $w + 150$ for the AC-UVW (11) and proposed CEP-UVW (46) models respectively. Both models appear to have comparable texture and noise extraction properties, even though staircasing has been reduced in the structure component $u = u_1 + u_2$ obtained from the proposed model. Here, we observe that staircase reduction does not affect either the texture removal properties of the G norm or the noise removal properties of the E norm. Parameters have been tuned in both models such that the L^2 norm of the texture (v) + noise (w) components are the same, $\|v + w\|_2 = 1057$.



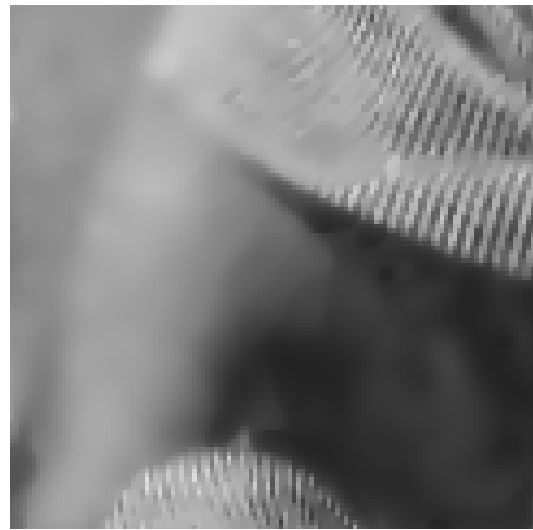
U : AC-UVW Model (11)



$U = U_1 + U_2$: CEP-UVW Model (46)



U : AC-UVW Model (11)



$U = U_1 + U_2$: CEP-UVW Model (46)

Figure 20: *Zoom-In, Structure Components U , $f = U + V + W$* : Left top and left bottom, zoom-in of the solution to the AC-UVW model (11). Right top and right bottom, zoom-in of the solution to the proposed CEP-UVW model (46). Staircasing, particularly on the left side of Barbara's face (her left) and arm, is observed in the components obtained from the AC-UVW model (11), while being reduced in the component obtained from the proposed model.



U_1 : CEP–UVW Model (46)



U_2 : CEP–UVW Model (46)

Figure 21: *The Discontinuous U_1 and Smooth U_2 Components Obtained from the Proposed CEP–UVW Model (46), $f = U + V + W$, $U = U_1 + U_2$.*